Mechanical eye stabilisation for robotic-assisted anterior segment surgery

Steven aan het Rot
Department of Biomechanical Engineering
Faculty of Mechanical, Maritime and Materials Engineering
Delft University of Technology, Delft, the Netherlands
stevenaanhetrot@gmail.com

Dimitra Dodou
Department of Biomechanical Engineering
Faculty of Mechanical, Maritime and Materials Engineering
Delft University of Technology, Delft, the Netherlands
d.dodou@tudelft.nl

Thijs Meenink
Preceyes BV
Eindhoven, the Netherlands
thijsmeenink@preceyes.nl

Maarten Beelen
Preceyes BV
Eindhoven, the Netherlands
maartenbeelen@preceyes.nl

***Abstract*—In the past two decades, robotic systems have been introduced to assist surgeons in improving the control of surgical instruments. To fully and safely utilise the potential of robotic precision, relative displacement and vibrations between the robotic system and the eye should be minimised. This study presents the design of an interface that mechanically fixates and stabilises the eye with respect to a robotic system, specifically to perform robotic-assisted surgery in the anterior segment.**

Fixation concepts are proposed to adhere the eye to interfaces based on friction, suction and insertion. A prototype is made and experimentally compared to evaluate their holding force while regulating a similar intraocular pressure for all interfaces for each concept. Based on the experimental results, suction is the most suited concept for eye fixation, with a holding force of 5 and 2.7 times than the insertion and friction, respectively.

Suction is implemented into two interfaces. To connect these interfaces to the surgical system, two connector concepts are researched and developed. Both interfaces combined with one of the connectors stabilised the eye with sufficient holding force while keeping the IOP within safe limits. Furthermore, placement in the surgical field, SI insertion, angle structure visualisation, and eye rotation was enabled.

***Index Terms*—Eye stabilisation; robotic-assisted surgery; ophthalmic surgery; surgical robotics.**

I. Introduction

Last year, over 300 million people were visually impaired around the world, it was estimated that 49.1 million were blind, and another 221.4 and 33.6 million had moderate and severe visual impairment, respectively [1]. For many of the eye diseases causing these impairments, surgery is often considered as the most suitable treatment to improve vision or to delay further visual impairment [2]. These intraocular procedures are associated with considerable challenges: tissue needs to be manipulated with high accuracy and precision, and instrumentation has to be held stationary for a prolonged duration [3], [4].

In the last 25 years, lasers have been introduced in anterior segment surgery to assist the surgeon with these complex tasks or replace conventional surgical tools. Laser-assisted procedures show excellent visual recovery and refractive results [5]. Nowadays, laser surgery is widely used and has become the technique of choice for most refractive surgical procedures [6]. To improve the procedural outcomes in these procedures, head movement is prevented by a headrest pillow and eye movement by eye fixation systems, often combined with eye-tracking [7]. In a visual fixation system, patients are asked to fixate their eyes on a light source or target to maintain their gaze at a constant position. In an eye-tracking system, a patient's eye is tracked to compensate for eye movement.

Laser surgery cannot be used for posterior ophthalmic procedures. Therefore, robotic systems have been introduced that can assist surgeons in improving the positioning of surgical equipment by compensating tremors, scaling motion, and introducing virtual fixtures [8], [9]. The challenge of these systems is ensuring a relatively unobstructed surgical field while providing high manoeuvrability and sufficient range of motion (RoM) to intraocular instrumentation [3]. Furthermore, robotic assistance comes at the cost of time [10], for example, due to motion scaling or set up time of the surgical system.

In recent years, clinical trials have been done using robotic systems in ophthalmic procedures, and at least one system has been commercialised [11], [12]. These trials indicate the potential of using robotic assistance: an improved surgical outcome, increased manoeuvrability and ergonomics, and a better learning curve [9], [13], [14].

To utilise the robotic precision at its full potential and within a safe environment, misalignment between the robotic system and (incision point of) the eye should be reduced as much as possible during a robotic-assisted procedure. Any voluntary or involuntary movement of a patient causes misalignment between the patient's eye and the surgical instrument (SI), which is connected to a surgical system. Accordingly, it is desirable to stabilise the eyeball [7], [15].

In robotic surgery, using the PRECEYES Surgical System (PSS), eye movements are minimised by stabilising the instrument insertion point. The virtual fixture or remote centre of motion (RCM) is aligned with the incision point using a

trocar and a trocar holder [10], [16]. The surgeon uses a SI at a second insertion point to stabilise and rotate the eye if needed. However, the eye is not fully constraining the rotation around the axis that intersects these points. Trocar fixation was sufficient for vitreoretinal surgery since the eye is in its resting position, the trocar is inserted perpendicular to the sclera, and instrument forces are mostly exerted in the posterior direction.

Until now, the PSS has been used to assist in retinal surgery. However, its precision can also be used in anterior segment procedures, which introduces other challenges. The eye needs to be rotated for an optimised reach of the anatomical structures and to be stabilised in an alternative way since the trocar does not constrain the rotation of the eye. Because in anterior segment surgery, trocar insertion and instrument forces are parallel to the corneal plane. Consequently, the instrument can slide with respect to the trocar in anterior segment surgery.

A visual fixation system in combination with eye tracking may be an alternative to make a surgical system responsive to small eye movements [17]. It already is considered as a feature for alignment of the RCM and the incision point [18]. However, eye motion can invalidate vision tracking algorithms, particularly at higher magnification when a SI is moved within the eye [16]. Furthermore, during procedures, such as minimally invasive glaucoma surgery, the surgical field is obstructed by a gonioprism. Consequently, eye tracking or eye fixation cannot be achieved [19].

Other alternatives to stabilise can be found in other ophthalmic procedures. In manual surgery, eye movement is limited by local or general anaesthesia, surgical equipment, or a combination. However, movements can still be introduced by changes in the depth of sleep [20]. Furthermore, Usage of surgical equipment may distort the eye, increase intraocular pressure (IOP), introduce extra discomfort for a patient, and often require one of the surgeon's hands [21]. In laser surgery, patient interfaces are introduced that use suction or compression to stabilise the eye without using the surgeon's hand. These interfaces are, for example, used for corneal flap cutting or docking an ophthalmic system onto the eye (applanation) [22]–[24]. Eye stabilisation interfaces have not yet been researched for robotic surgery.

In summary, to optimise surgical performance in robotic-assisted surgery, misalignment between the robotic instrument and the eye should be minimised. The current stabilisation technique is not adequately suited for robotic-assisted anterior segment surgery. Because of the obstructed field in some anterior segment procedures, a software-based eye-tracking system seems unattainable. The research question that arises is: *What are the design characteristics for an interface that mechanically fixates and stabilises the eye to perform anterior segment robotic-assisted surgery?* This interface should best meet the imperatives of docking a robotic system onto the human eye.

This study will first provide the necessary background information about anatomical structures and the preceyes surgical system. Hereafter, in the global design section, three different concepts are introduced. Three prototypes are developed to compare the concepts in an experiment. The most suited concept is selected for a detailed implementation in the surgical system. Detailed requirements are listed, and again concepts and prototypes are developed. The prototypes are experimentally verified in three different experiments. Finally, the last sections will provide a general discussion containing recommendations for future research and designs, followed by a conclusion.

II. Background

A. Eye anatomy and terminology

The relevant anatomical eye structures for eye fixation are the conjunctiva, the sclera, and the cornea. The conjunctiva is the most outer layer and keeps the eye surface moist and lubricates and protects the eye from dust and infections. The cornea is the transparent layer in front of the iris, allowing light to enter the eye. The sclera is the white connective tissue of the eye with a thickness varying from 0.3 mm to 1.0 mm. The intersection of the sclera and cornea is called the limbus [25], [26].

The anterior segment of the eye consists of an anterior chamber, the part between the iris and the cornea, and a posterior chamber, the part between the iris and the lens. These chambers are filled with aqueous humour, a clear watery fluid, which transports nutrients to the eye. Aqueous humour is produced by the ciliary body, flows through the iris, and exits through the trabecular meshwork and schlemm's canal into the eye's circulatory system [25], [26]. The anatomical structures and aqueous flow (brown arrow) are presented in Figure 1.

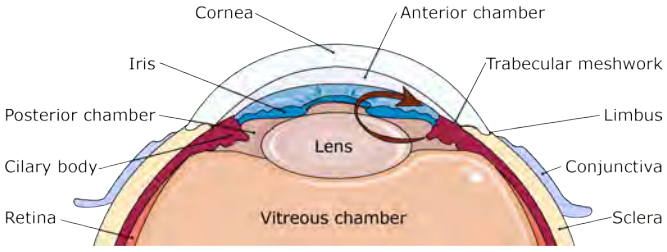

Fig. 1: Cross-sectional representation of the anterior segment of the eye (adapted figure [27])

Aqueous humour and vitreous humour in the vitreous chamber ensure the round shape of the eye is maintained. The aqueous humour maintains the intraocular pressure (IOP). When the production and drainage of the aqueous humour are equal, the pressure is stable and usually 10-20 millimetres of mercury (mmHg), where 1 bar is 750 mmHg. When an imbalance exists between production and drainage, the eye pressure can become too high (hypertension), which may lead to optic neuropathy (damage to optic nerve), a reduction in vision, or even blindness [28]. The parthenogenesis of glaucomatous optic nerve damage is a complex neurological system and is still not fully understood. Oxidative stress is involved, caused by unstable blood flow due to fluctuating IOP or unstable auto-regulation [29].

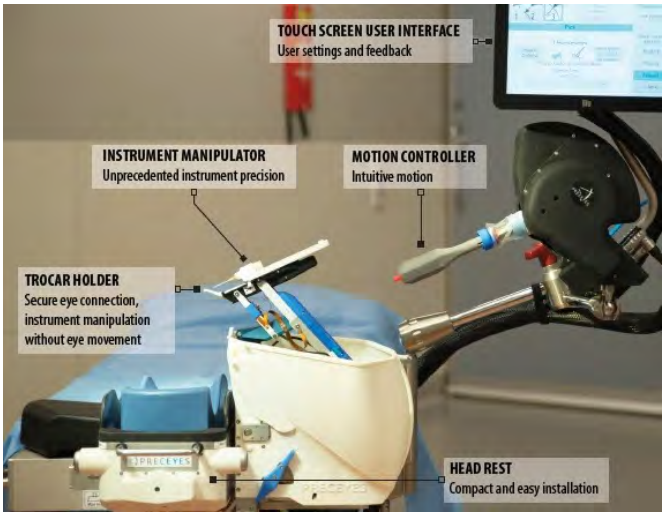

(a) General layout [11]

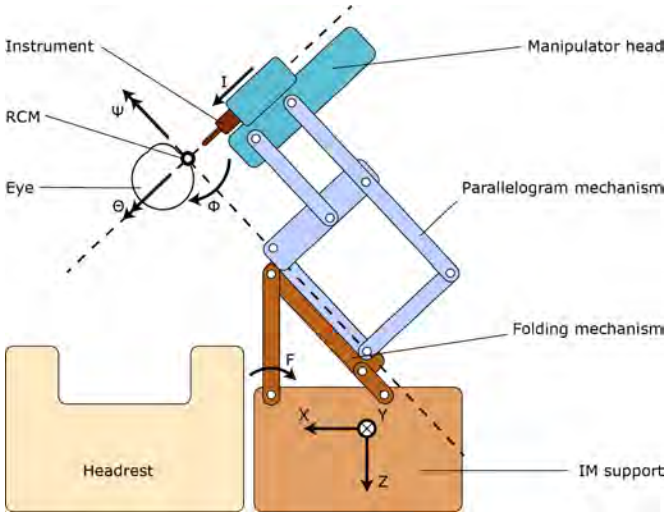

(b) Degrees of Freedom (Y into paper)

Fig. 2: Preceyes surgical system

B. Preceyes surgical system

The surgical system used in this study is the PSS shown in Figure 2a. The PSS is a medical robot developed for vitreoretinal surgery and designed by Preceyes B.V with an accuracy of less than 20 micrometres.

The input joystick is controlled by a surgeon and manipulates the movement of the instrument manipulator (IM) to which a SI is connected. The motion provided by the surgeon is scaled and filtered to provide better precision and stability. The PSS is rigidly secured to a headrest and aligned to the surgical incision. The instrument manipulator design is based on a parallelogram mechanism which provides a mechanical RCM (Figure 2b). The system uses counterweights to enhance stability and safety, minimise joint torques, and hold the system in a fixed orientation in the event of a power loss or system failure [3], [10], [30].

The PSS has eight Degree of Freedom (DoF), introduced by the instrument manipulator (IM), a remote centre of motion positioner (RCMP), and a folding mechanism. The IM consists of a parallelogram mechanism that provides two side rotations (Ψ and Φ) and an IM head that provides the translation in and rotation around the instrument axis (Θ and I), and a rotation about that axis (I). These DoFs rotate or translate the instrument axis around or through the RCM.

The RCMP introduces three DoF to the IM support to position the RCM: translation along with the X-, Y-, and Z-axis with respect to the headrest (shown in Figure 2b).

An extra DoF is introduced to facilitate folding back the IM, ensuring quick-releasability (F). The system folds over an arc, first translating in the X direction and then in the Y.

III. Global design

In this section, the global design of different fixation interfaces is presented. First, global requirements will be set for such an interface. Hereafter, three fixation principles and their design variables are introduced. Three prototypes are designed, corresponding to the three principles to compare these principles in an experiment.

A. Global requirements

1) Functional: To enable the PSS to operate, an interface shall hold the eye at a fixed position with respect to the RCM of the robot. The interface must be able to suppress forces introduced by eye movements and instrument manipulation. Finally, For an optimised reach of the PSS in the anterior segment, the eye shall be rotated up to 20 degrees.

2) Procedure: The interface shall be placed onto the available surgical field while enabling anterior segment surgery with the PSS. A SI shall be inserted to perform such a procedure and have sufficient RoM to manipulate eye tissue. An unobstructed surgical field shall be needed to visualise tissue with optical equipment.

3) Safety: Eye fixation cannot induce any other visual impairment. Forces and the IOP have to stay within safe limits, and the PI shall not detach during surgery. These limits will be presented in subsubsection III-C1.

B. Eye fixation concepts

Based on the fixation devices currently used, three promising concepts come forward. The instruments used as inspiration are fixation rings, suction rings, and trocars. These lead to three concepts: friction, suction, or insertion.

1) Friction: The friction concept is based on fixation rings currently used in manual surgery. The friction force is increased as the compression force is increased. The tribology

of soft biological interfaces is often dependent on complex interactions between components. [31].

The compression force pushes the eyeball into the orbit while acting as a mass-spring-damper due to the fluid inside the eye and its muscles. The eye "pushes back" the PI. Consequently, the eye is pressurised, and the IOP is increased [32].

The coefficient of friction of the conjunctiva and cornea have been experimentally determined and are dependent on both the grasping surface and the lubricant (mucus or human tears). Consequently, measurement results differ among studies due to the different grasping mediums and artificial lubricants used [31], [33].

2) Suction: Suction cups are used in laser surgery to stabilise the eye. It is based on the pressure difference between the 'gripping' area and the ambient pressure (usually around 1 bar). When a suction cup is docked to a surface, air is sucked out of the cup, which creates a low-pressure volume. The atmospheric pressure presses from the other side, resulting in a suction force that depends on the pressure difference and the contact area ($F = \Delta PA$). This relation is used to estimate suction forces for patient interfaces [34].

As a result of the suction applied to the sclera, the sclera deforms as shown in Figure 3, and as a consequence, the IOP increases. Although the rise in IOP is a side effect, it has been used advantageously. For example, to have a stable and solid cornea during microkeratome flap cutting or compensate for IOP loss during intraocular procedures.

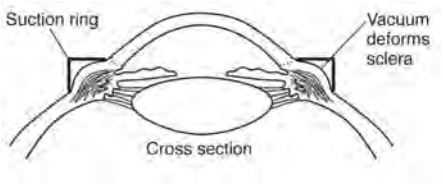

Fig. 3: Scleral deformation due to suction pressure [35].

3) Insertion: The last concept is based on insertion. For intraocular surgery, the anterior or posterior chamber is reachable by penetrating the sclera or cornea. Stabilising this point of insertion is done by, for example, trocar used in the PSS [10]. The trocar fixation concept can be used in an interface in which only the tip of the needle partially penetrates the sclera. However, instead of using one point, a surface is filled with tiny needles on the entire surface.

C. Design of fixation prototypes

1) Design variables: The PIs have to fit onto the eye corresponding to the dimensions shown in Table I. Dimensions of porcine eyes are included since porcine eyes are used in the experiments. Porcine eyes differ slightly from human eyes [36], [37].

The eye's dimensions determine the dimensional parameters for the ring interface placed on the eye: the outer and inner diameter (OD and ID). Consequently, the contact area can be calculated using Equation 1.

TABLE I: Dimension porcine and human eye

	Human eye	Porcine eye
Visible iris (VI)	10.6 to 11.7 mm	12.0 to 14.3 mm
Eye diameter (ED)	24 mm	23.9 mm
Corneal diameter (CD)	15.5 mm	16.9 mm

Similarly, the suction area can be calculated using the suction diameter (SD). The final dimensional parameter is the diameter of needles used for the insertion concept. The dimensions of the eye and dimensional parameters of the interfaces placed on the eye are presented in Figure 4.

$$dA = r^2 \sin(\theta) d\theta d\phi \tag{1}$$

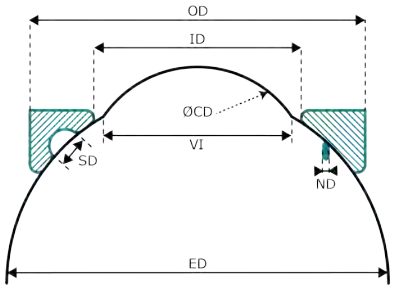

Fig. 4: **Dimensional parameters**: outer, innner, suction, and needle diameter (DR, ID, SD, and ND). **Eye dimensions**: visibile iris (VI), corneal and eye diameter (CD, and ED) [36], [37].

A limit is set for the IOP at 50 mmHg to prevent optic neuropathy. An IOP of 50 mmHg impairs the optic nerve oxygenation selectively, without affecting the blood supply to the eye [38]. The limit is based on the mean ocular perfusion pressure (OPP): the difference between the IOP and the brachial blood pressure [39], [40]. The amount of optic nerve damage is dependent on time and pressure. However, within safe limits, axonal transport abnormalities are reversible (for perfusion pressures of over over 25 mmHg) [41]. For example, no significant difference are found in axonal transport for 3 hours of IOP elevation from 10-15 to 40-45 mmHg [42], [43].

Finding the optimal vacuum level guaranteeing a tolerable IOP and sufficient stability for a safe surgical procedure is crucial [44]. Common suction pressure (P_S) range from 300 to 700 mbar [34], [45]. However, no concrete clinical recommendation for surgeons exist with respect to which vacuum is safe [46].

The upper limit of compression force (F_C) exerted parallel to the optical axis is 300 mN and based on ophthalmic surgeons feedback [32]. 300 mN is considered to be adequate to immobilise the eyeball, suppress vibrations, and involuntary movements [32]. The local pressure on the sclera is dependent on the F_C and the contact area. For example, A smaller contact area with a similar compression force would result in higher local pressure on the sclera.

The upper limit of the scleral force (F_S) is 120 mN and based on freehand experiments done by surgeons [24].

The holding force (F_H) should be at least 250 mN. The limit is based on extraocular muscle forces and forces due to tool manipulation. The maximum for the forces exerted on tissue in ophthalmology procedures is 50 mN [47]. The force due to the muscle forces can be calculated by ocular motor properties (0.5-0.99 g/degrees). The upper limit for eye rotation is 20 degrees. Consequently, the maximal force due to the extraocular muscles is 200 mN [48], [49]. Similar eye muscle properties are found when local, eye-drop anaesthesia is used [50].

TABLE II: Limits for design variables

Variable	Limit	Reference
PI dimensions	Dimensions presented in Table I	[36], [37]
Intraocular pressure	$IOP \leq 50$ mmHg	[41]–[43]
Suction pressure	$300 \geq P_S \leq 700$ mbar	[34], [45]
Compression force	$F_C \leq 300$ mN	[32]
Scleral force	$F_S \leq 120$ mN	[24]
Holding force	$F_H \geq 250$ mN	[47]–[50]

2) Prototype development: A prototype is made for each concept to compare the presented concepts experimentally using porcine eyes. As such, the dimensions of the prototypes are fitted to the dimensions presented in Table I. The dimensions and calculated contact or suction area for the different prototypes are presented in Table III. A cylindrical hole is added to connect each prototype to the test setup and allow rotation around the optical axis. These prototypes are presented in Figure 5 and are printed using an HP 3D MJF printer in polyamide 12 (PA12), which is a biocompatible material.

TABLE III: Dimensions of fixation prototypes

	Concept			
	ID [mm]	OD [mm]	SD [mm]	Contact or suction area [mm^2]
Friction	13	20	-	173
Suction	13	20	3.8	214
Insertion	13	22	-	242

The friction prototype has a contact area with 18 gripping teeth distributed over 320 degrees around the optical axis. The teeth have a height of 1 mm. The remaining 40 degrees is left open to enable SI insertion.

The suction prototype consists of a vacuum chamber connected to a Luer slip fitting to connect suction tubing. The suction area has an oval shape to provide an opening for SI insertion. The oval consists of two halved rings with 10 degrees of revolved extrusions in between.

The insertion prototype consists of six general 27Gx1" needles fixated into a 3D printed housing. These needles are inserted into the conjunctiva and sclera at 2,5 mm from the limbus. The scleral thickness for medium-sized pig eyes at 2,5 mm from the limbus is approximately 0.7 mm [51]. Since the needles are inserted at an angle, the sclera in the insertion direction is approximately 0.9 mm. Consequently, the insertion depth is set at 0.7 mm and is designed to not (fully) penetrate the conjunctiva and sclera. After manufacturing, adjustments were made to provide an opening for SI insertion.

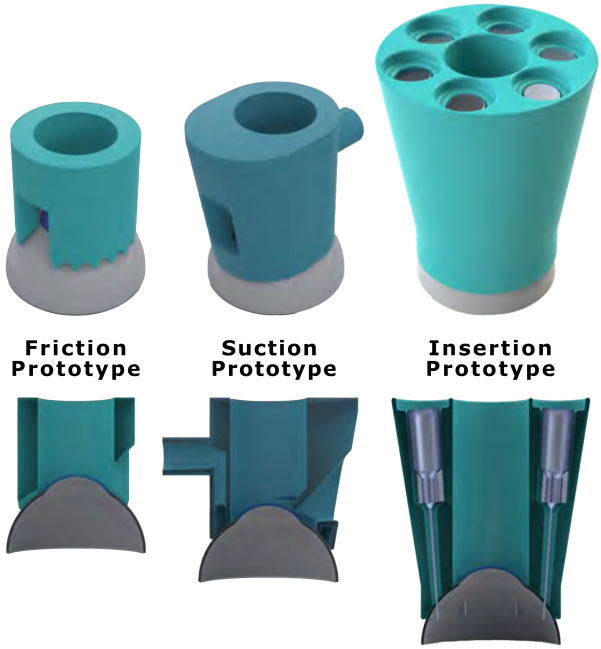

Fig. 5: Patient interface prototypes

D. Experimental comparison fixation prototypes

In this section, an experiment is presented which compares the concepts presented in the previous section. First, the purpose and method of this experiment are presented, followed by the results and discussion.

1) Purpose

This experiment aims to quantify and compare the performance of the suction, insertion, and friction PIs.

The break-away force (BAF) is chosen as the performance metric to compare the three principles. The BAF is the force needed to rotate the eye, causing the eye to break away from the prototype. The BAF imitates the forces generated by the eye muscles by exerting force approximately 12 mm from the eye's centre of rotation (CoR). The BAF performance does not take all global requirements into account. Still, it presents a basis to compare which principle is suited to stabilise the eye.

All eyes are pressurized to the same IOP (20 mmHg) before placement of the PI. Hereafter, the IOP is increased to 30 mmHg by adjusting the F_C for all principles and P_S for the suction principle. These variables are independent and are set using actuators, weights, or other machinery. The dependent variables: IOP and BAF are measured during the experiment and and F_S is calculated. All variables are presented in Figure 6.

The hypothesis is that the suction principle will have the highest BAF when each prototype is set up with a rise in IOP of 30mmHg. For a suction pressure of 300 mbar, the suction force will be 6.42 N, where the compression force has an upper limit of 300 mN for the friction and insertion concepts. Furthermore, the insertion principle will outperform the friction principle because of the needles.

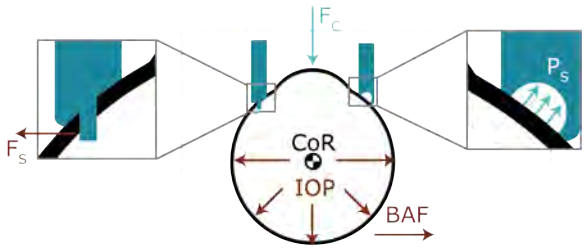

Fig. 6: Independent (blue) and dependent (red) experiment variables for different PIs.

2) Method The setup was based on a traditional tensile test setup. However, instead of a linear translation, the setup facilitates a rotation of a porcine eye by exerting a pull force at a fixed distance to the CoR. An overview of the setup is presented in Figure 7 and in more detail in appendix A-1.

The setup begins with the eye holder (light blue) placed onto two standing bearings, which allow the eye to rotate about an axis aligned with the eye's CoR. Usually, the eye's has three DoF. However, the eye was allowed only to have one rotational DoF.

The eye holder was pulled by a linear micro-stage (PT1/M-Z8 25 mm Thorlabs) to initiate the rotation (blue). The pulley fixed to the eye holder ensures a constant distance to the pull force (12 mm). Therefore, the resulting torque was directly proportional to the pull force. The linear stage was placed horizontally to keep the setup compact, and the height creates a distance between the micro-stage and 'wet' components. Finally, a calibrated load cell (LSB200 Futek) was connected to the micro stage to measure the pull force.

A linear guide rail (M12H9 Fafeicy) was used for placement of the PI (brown & dark blue)) which removed 5 DoFs, allowing the PI to only translate in the normal direction of the rotation. A 3D printed docking was used to connect the PI to the linear guidance. The docking also allowed for the placement of (counter)weight to regulate the F_C. P_S was regulated using a vitrectomy function of an Alcon Accurus connected to the PI via tubing (yellow).

To regulate the initial IOP, a height-adjustable column was used filled with a balanced salt solution. To measure the IOP, a calibrated pressure transducer was used (RS-PRO 828-5713). The cannula inserted into the eye was connected to the column and transducer using a three-way tap (purple).

All components are connected to an aluminium frame (grey). Data acquisitors and NI LabVIEW were used to acquire the data from the sensors to a computer. For control of the micro-actuator, a K-Cube Servo Motor Controller and Kinesis Software are used.

The protocol consisted of 4 steps, excluding preparation and cleaning (Figure 8a).

1. Porcine eye placement A porcine eye was placed in the eye holder using styrofoam and sewing pins (Figure 8b). The eye holder with the porcine eye was installed in the test setup.

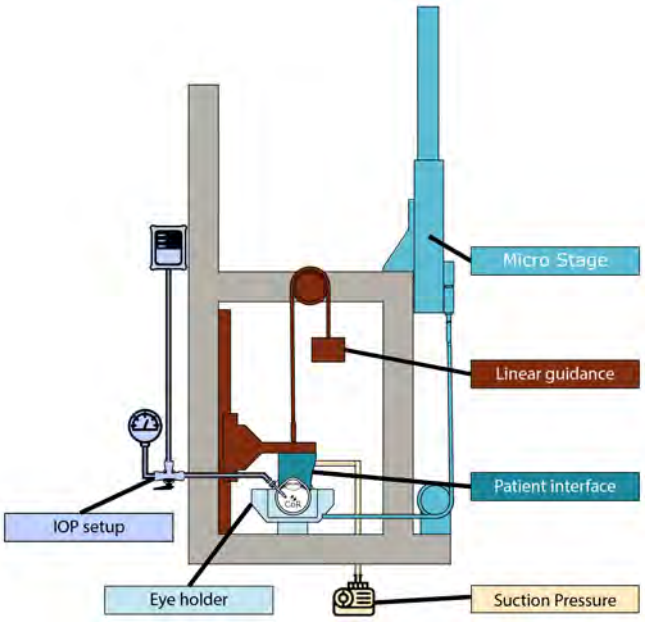

Fig. 7: Overview of Experimental setup

2. Set IOP at 20 mmHg The porcine was inserted intravitreal with a trocar in the pars plana at 4 mm of the limbus in the direction of the centre of the globe [23], [44] (Figure 8b). A cannula was inserted in the trocar and connected to the transducer via a three-way tap. The data was acquired in LabVIEW with a loop time of 50 ms. The syringe was set at the height of 272 mm to set the IOP at 20 mmHg (26.66 mbar) [46]. Hereafter, the tap was turned to have a closed-loop between the transducer and the eye.

3. PI application After the eye is pressurised, the PI is connected to the docking. The F_C and P_S are regulated, corresponding to a rise in IOP of 30 mmHg (Total IOP is 50 mmHg). The F_C was set using weights and pulley's to get a constant F_C (Table IV & Figure 8c). . The P_S was regulated at 320 mbar (Figure 8d).

4. Micro-stage actuation Next, the micro stage was actuated. The velocity was set at 0.3 mm/s, the max acceleration at 0.15 mm/s ^{2}, and the moving distance at 5-15 mm. The micro-stage movement initiated a measured pull force to the eye holder, resulting in torque around the CoR. Consequently, the eye broke away from the porcine eye.

After the measurements, the raw data was processed in Matlab. The IOP value was converted from mbar to mmHg, and the events and relevant data points were determined and obtained

TABLE IV: Compression force and suction pressure for PI application

	Friction	**Suction**	**Insertion**
Compression force	1074 mN	296 mN	1091 mN
Suction pressure	-	320 mbar	-

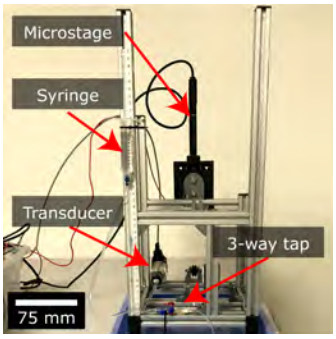

(a) Test setup with sensors, actuator, and syringe connected

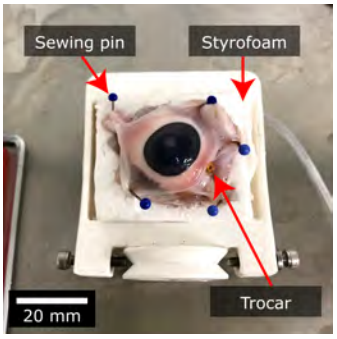

(b) Eye in holder with styrofoam, sewing pins, and trocar

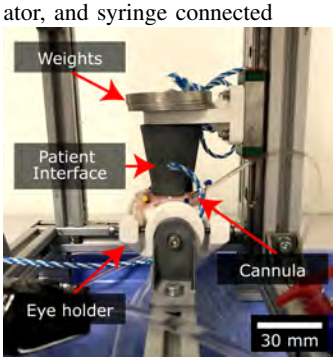

(c) PI setup with extra compression force

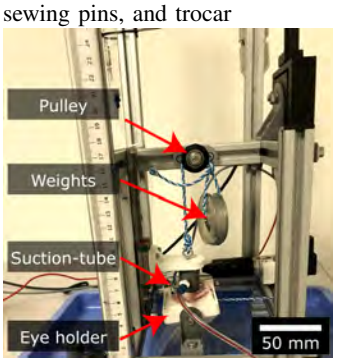

(d) PI setup with counterweights and suction tubing

Fig. 8: Suction PI setup (scales are indicative)

(presented in appendix A-2). The events distinguished in the data were the PI application or eye rotation induced by micro-stage actuation.

The data showed a drop in the force data when the PI broke away from the eye. However, a plateau was observed in the insertion and friction measurements instead of a drop. Consequently, The force was noted when a PI broke away to prevent data processing errors because the break-away moment was difficult to distinguish.

A stress concentration factor was used to calculate and estimate the F_S for the insertion prototype. Each needle punched a little hole into the sclera/conjunctiva. The BAF is considered to be equally distributed among the six needles. Consequently, the maximal F_S can be estimated roughly by multiplying the force with a factor 3 corresponding to the stress concentration factor commonly used for holes.

3) Results

Sixteen porcine eyes were used in the experiment, resulting in 13 force measurements for all prototypes (*N=13*) and *9, 10 and 8* IOP measurements for the friction, suction, and insertion concepts, respectively (*N=9, 10 or 8*).

The data points and boxplot obtained from the raw data are plotted in Figure 9. The calculated mean and standard deviation are presented in Table V. Individual data for each measurement is presented in appendix A-3.

In Figure 9 and Table V a clear difference between the prototypes was observed. Suction had the highest break-away force (BAF_{mean}= 7.51 N) and friction the lowest (BAF_{mean}= 1.54 N), leaving the insertion interface in between (BAF_{mean}= 2.81 N). Furthermore, the suction BAF data dispersion was the highest, while the friction and insertion force data were more clustered. Finally, the mean F_S was estimated to be 1405 mN.

TABLE V: The Mean and standard deviation of measured data

	Friction		Suction		Insertion	
	BAF (N)	**IOP (mmHg)**	**BAF (N)**	**IOP (mmHg)**	**BAF (N)**	**IOP (mmHg)**
Mean	1.54	49.33	7.51	47.70	2.81	50.38
SD	0.48	6.12	2.20	4.71	0.76	9.71
N	*13*	*9*	*13*	*10*	*13*	*8*

For the IOP data, the dispersion was the other way around. The IOP data showed the rise in IOP to be approximately 50 mmHg for all PIs. With slight differences between the concepts ($<$ 3 mmHg). One outlier was observed in the IOP data for the insertion interface at 72 mmHg.

In some cases, the rise in IOP due to PI application was not measured due to the lack of backflow of the balanced salt solution. The lack of backflow could be solved by doing another set of measurements, replacing the trocar or cannula, or replacing the PI. IOP values are excluded when this was not solved. Resulting in four, three, and five values that are excluded for the friction, suction, and insertion interface, respectively (N=9, 10, or 8).

Furthermore, the micro-stage was given an extra displacement at four suction interface measurements because the initial displacement was insufficient. The short pause in actuation resulted in a drop in IOP and Force, but the extra displacement ensured the eye to break away.

4) Discussion

The boxplot Figure 9 shows the IOP was successfully increased to approximately 50 mmHg, and the linear micro-stage successfully pulled the eye holder. Consequently, the PIs rotated and broke away from the porcine eyes. Further discussion of results is divided into four sections: concepts, measurement setup, procedure, and data processing.

For both the compression and suction concepts, similar values for the rise in IOP are found in other articles, indicating the correctness of the IOP data [32], [44]. For example, an increase of IOP from 20 mmHg to 45.18 ± 4.34 mmHg can be found that corresponds to a P_S of 350 mbar [44], although the suction area has not been given. Furthermore, a rise in IOP of 4.67 mmHg can be found corresponding to an F_C of 178.3 mN [32]. Linear extrapolation of the F_C to 1074 mN results in a rise in IOP of 28.1 mmHg.

The F_C used to pressurise the eye to 50 mmHg exceeded the F_C limit. A lower F_C is likely sufficient to fixate the eye at a 20-degree rotation since the BAF values found were more than three times the necessary F_H,

The F_S for the insertion prototype is estimated at 1405 mN and thus exceeded the boundary of 120 mN [24], which would be a reason to reject the insertion interface as well. However,

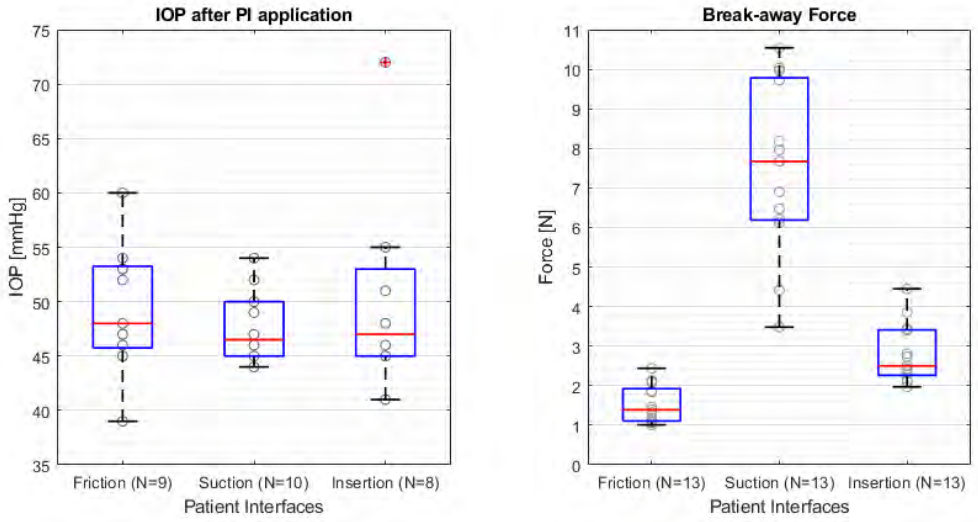

Fig. 9: Individual data points and boxplot of results break-away force measurements

since F_H is divided among the needles used, the F_S can be decreased when more needles are used. Moreover, the holding force needed for eye fixation (250 mN) is significantly lower than the mean BAF (2810 mN).

The estimated suction force of 6.85 N corresponds to values found in literature determined by pulling of the interface along the optical axis [46], [52]. However, comparing the BAF to values in literature is not possible since the experiment shown is the first of its kind. The BAF values found all are higher than the compression or suction forces exerted by the PIs, which could be because soft tissue is used, and the prototypes are form-locking the cornea that is 'sticking out'. Furthermore, the distance from the PI to the rotation axis of the eye holder may have been more than 12 mm. Consequently, the BAF measured may have come out higher. Nevertheless, a comparison can still be made.

The BAF data shows an explainable difference between the prototypes. The suction interface attaches best to the eye, and the insertion interface outperforms the compression interface.

The design parameters of the prototypes are intervening variables affecting the F_C, F_S, rise in IOP, and BAF. Although the insertion and friction prototype have different contact areas, the rise in IOP for a similar F_C is comparable. The rise in IOP is not affected by a smaller contact area of the friction prototype despite having a higher local pressure on the sclera. However, a smaller suction area for the suction concepts would affect the rise in IOP. For example, a smaller suction area would mean less rise in IOP, a lower suction force, and a lower BAF.

The experimental setup had several locations in which misalignment could occur. For example, the place of the pulleys is significant for the force measured by the load-cell or exerted on the PI. The position of these pulleys are adjustable to minimise misalignment and use small-angle approximation is throughout the experiment.

During the procedure, the measurement of the IOP showed a small and continuous loss in IOP, which may be introduced by a leakage induced by a 3D-printed connector in the IOP setup or IOP perspiration of tissue. In other literature, a decrease in IOP is seen as well [45], [53].

The IOP leakage does not likely affect the IOP results since it is measured immediately after setting up the initial IOP. As mentioned before, the IOP after PI application corresponds to data from other literature. However, it could have affected the BAF and IOP later during the measurement. The IOP always stayed relatively high (more than 40 mmHg), and the eye never became soft or limp during testing. The BAF results shown are barely affected by the leakage. Even if the drop in IOP affects the BAF, the error is systematic for all measurements, and a comparison can still be made.

The actual P_S at the PI is not measured in the experiment. The actual pressure may be lower than the pressure regulated with instrumentation [46]. A lower actual P_S would result in a lower suction force and BAF. Therefore, a suction interface with an actual P_S of 320 mbar would likely provide a higher BAF.

The test setup allowed only one DOF for the porcine eye: a rotation around the CoR of the eye. This is considered simplification is sufficient to mimic the rectus muscles of the eye.

Installing and removing the eye holder containing the styrofoam and porcine eye introduces a random error and causes dispersion of the data. Each time the eye holder is removed and installed, the alignment between the PI and the porcine eye is slightly different.

The porcine eyes used in these experiments came out of the freezer and first had to be thawed. These eyes were not used before and frozen at a temperature of -20 °C. Storing tissue in a freezer has been a common practice since the 1950s and probably has only a small effect on the eyes. Furthermore, freezing and thawing lead to insignificant changes in tissue stiffness for scleral tissue [57].

5) Conclusion

The hypothesis presented at the beginning of this section can be accepted. When proper alignment is provided, the suction prototype outperforms the other prototypes, providing the highest holding force and no compression force is needed (except for PI application). Furthermore, the friction prototype underperforms with respect to the other concepts. An interface based on insertion could be promising when it is further developed. Usage of the friction needs a compression force exceeding the limit and is, therefore, less suited for eye fixation. To conclude, suction is the most suited concept for eye fixation based on the difference in performance. a

IV. Detailed design

The second part of the study will provide the detailed requirements, concepts, and design of a patient interface (PI) and its connection to the surgical system. The PI will be implemented in the PSS and designed for usage within anterior segment procedures. Three experiments are presented to verify if requirements are met or performance is reached to validate the concepts.

A. Detailed requirements

In interaction with surgeons and engineers, the list of detailed requirements is made and presented in Table VI. The requirements are based on the surgical system, anterior segment procedures, and design variables' limits.

B. Suction and connection concepts

1) Suction interfaces: The suction interface is further developed into different shapes to enable SI insertion. Two concepts are proposed: a U-shaped patient interface (U-PI) with an open end and an oval-shaped interface patient (O-PI).

2) Connectors: To ensure the PI is connected to the PSS, several connections are considered. The PI can be connected to the headrest (HR), IM support (IMS), the IM after the folding mechanism (IMF), or the IM Head (IMH) (Figure 10).

HR-connector The PI is connected to the HR (presented in Figure 10a). The HR concept has the largest force loop of these concepts. To ensure the PI and RCM are aligned, three translations (X, Y, and Z) must be implemented. To allow for the rotation of the eye, another DoF has to be added using a joint or a 4-bar mechanism in which the eye's CoR functions as one of the hinges of the 4-bar. In both cases, the rotation of the eye has to be actuated. Furthermore, an additional mechanism has to be implemented to make the PI quickly releasable.

IMS-connector The PI is connected to the IMS (presented Figure 10b). The IMS concept has no DoF between the PI and RCM since it is directly connected to the RCMP. To rotate the eye, the PI has to rotate around the RCM to maintain alignment. The PI stays at its position while the system is folded back. Therefore, an additional mechanism needs to be implemented to ensure a quick releasable system.

TABLE VI: List of surgical system, procedure, and safety requirements (SSR, PR and SAR)

	Requirement	**Rationale**
	Surgical system	
SSR1	The PI shall be able to rotate at least 10 and at most 20 degrees in the medial direction relative to the eye's resting position	For an optimised reach of the PSS in the anterior segment, the eye may need to be rotated up to 20 degrees.
SSR	The PI shall hold the eye at a fixed position with a holding force of at least 500 mN	According to the minimal holding force defined in subsubsection III-C1 multiplied by a safety factor of 2.0
SSR3	The maximum displacement of the eye with respect to the RCM shall be 25 µm at most during stable docking of the PI.	Similar to the accuracy of the surgical system of Preceyes and shall provide sufficient accuracy for anterior segment surgery based on the width of the trabecular meshwork: 50-150 μm [54]
	Procedure	
PR1	The PI shall allow for insertion of a SI into the eye's anterior chamber at the RCM	During anterior segment surgery, the surgical system will insert a SI through the incision point of the eye, which is aligned with the RCM.
PR2	The PI shall enable placement of a gonioprism and provide a clear path for visualization with a microscope.	The Preceyes surgical system is a telemanipulation system. Therefore visual feedback is needed to control the surgical robot.
PR3	PI shall be placed within the surgical field defined by human eye dimensions, speculum properties, and eye rotation.	The PI shall fit according to the eye dimensions presented in Table I. Furthermore, it shall be placed in the surgical field between the eyelids, which is constrained by the palpebral fissure height of ± 30 mm and speculum properties: the blade width of 15-20 mm and blade spread (BS) of 20-35 mm [55], [56].
PR4	The PI and its connection shall provide the IM with sufficient RoM to rotate the SI to enable anterior segment surgery (20 degrees around Φ and 120 (± 60) degrees around Ψ).	The RoM is defined experimentally to realize anterior segment surgery using the surgical system.
	Safety	
SAR1	The IOP shall stay below 45 mm	5 mmHg lower than upper limit presented in subsubsection III-C1
SAR2	The suction pressure shall stay between 300-700 mbar.	According to subsubsection III-C1
SAR3	IM shall remain quick-releasable within 2 seconds	Currently, the Preceyes surgical system is quickly releasable in two seconds. Which shall not be affected by the PI.
SAR4	Components of PI shall be quickly releasable within 2 seconds	The PI is placed on the patient's eye and shall be quickly releasable. The time and moment depends on the system integration and shall be 2 seconds at most.

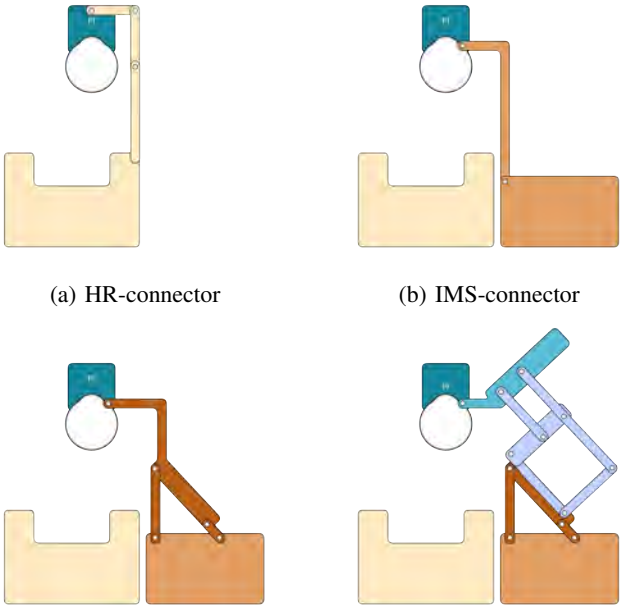

(a) HR-connector (b) IMS-connector

(c) IMF-connector (d) IMH-connector

Fig. 10: Connector concepts

IMF-connector The PI is connected to the IMF stage (presented Figure 10c). The IMF concept is similar to the IMS concept, with one extra DoF between the PI and RCM (F). Consequently, the PI is retracted together with the rest of the IM.

IMH-connector the PI is connected to the instrument manipulator head stage (presented in Figure 10d). The IMH concept has two rotational DoF (Φ and Ψ) between the PI and RCM and must allow these DoFs to ensure the PSS can be used. Therefore, a spherical joint, universal joint or something similar has to be implemented. However, implementing two DoFs within the design envelope is complex. Since this concept is connected to the IMH, it retracts along with the rest of the IM.

To constrain the eye to the PSS, the number of DoF to be implemented for the HR-, IMS-, IMF-, IMH- connectors are 5, 2, 1, and 2, respectively. The more DoF the PSS-PI loop requires the more complex the concept will be. These DoFs must be implemented in a limited design space due to the visualisation and RoM required for the IM. Furthermore, the accuracy decreases when more DoFs are implemented between the PI and PSS.

The IMS- and IMF-connector are considered most suited for implementation with the PSS because of the complexity of the other connectors. The HR-connector needs a enable a considerable amount of DoFs, at the expense of alignment between the PI and RCM. Furthermore, implementing the two DoFs of the IMH-connector in the limited designing space will result in less RoM or accuracy. More elaborate considerations per requirements are given in appendix B-1.

C. Design of suction and connection prototypes

The design of implemented interfaces consists of two suction interfaces and two different connectors.

1) Suction Interfaces: The designs of the U-PI and O-PI are presented in Figure 11. Both designs have an ID, OD and SD of 13, 22 and 2.75 mm as presented in Table VII. The dimensions shown are chosen such that the PIs both fit within the surgical field defined by the eyelids and speculum. The U-PI interface consists of a halved ring and two 35 degrees revolved extrusions. At the side at which instrumentation is inserted, no material is added. The O-PI consists of two halved rings, separated by two revolved extrusions of 20 degrees to enable space for surgical instrumentation insertion. Consequently, the suction areas can be calculated using Equation 1.

	Concept			
	ID [mm]	OD [mm]	SD [mm]	Contact or suction area [mm^2]
U-PI	13	22	2.75	104
O-PI	13	22	2.75	166

TABLE VII: U-PI and O-PI dimensions

The designs also allow for docking a gonioprism (Volk Single Use 4-Mirror Gonio Lens), which make it possible to visualise the angle of the anterior chamber. The interface also incorporates a male Luer slip fitting to connect suction tubing. Finally, the axis through the small rings, placed symmetrically, are aligned with the RCM.

2) Connector: The connectors are presented in figures 12 and 13 and both have a design that consists of an O shaped design at the lower part and a curved triangular design connected to a halved ring at the upper part. These shapes are a consequence of SSR1, PR2, and PR4, resulting in the three constraints:

1) The connector shall be designed around the patient's head,
2) The connector shall provide the necessary space for RoM of the IM, insertion of the SI and an unobstructed path for visualisation with the microscope and gonioprism.
3) The connector shall not intervene with the PI placed onto the eye.

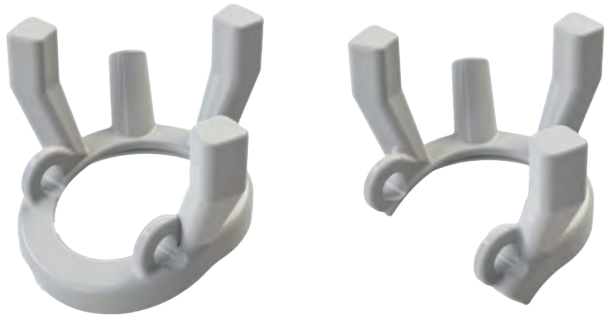

(a) O-PI (b) U-PI

Fig. 11: Suction Patient Interface prototypes

The two pins at the end of the connector are designed to be snap-fitting to the PIs. Below the curved triangle, both designs have an O-shaped design, providing space for the Ψ-actuation assembly of the PSS. The exact size of these O-shapes is dependent on where the designs are connected. The IMF-connector is bolted to a small surface available on the IMF-stage. The IMS-connector is connected to threads already available on the IMS-stage. To prevent the designs from rotating around the axis going through these fixation points, the IMF-connector is given a fork-like design, and the IMS-connector is connected with three bolts.

A FEM analysis is performed to optimise the strength and stiffness as presented in appendix B-2, which resulted in the design having thickened ribs. The connectors are fixated at the bolted locations, and the force is exerted at the pins at the end. The maximum displacement is kept below 0.3 and 0.6 mm, and the stresses are well below the yield stress for the IMS- and IMF-connectors, respectively. The total exerted was 500 mN, and the material used was PA12, which has a flexural modulus of 1730 MPa and tensile strength of 48 MPa [58].

(a) Design (b) Integrated into system

Fig. 12: IMF-connector

(a) Design (b) Integrated into system

Fig. 13: IMS-connector

D. Bench test

A bench test is performed to test the requirements, which does not need an ex vivo eye and does not need a sterile barrier.

1) Purpose

The purpose of the experiment is the verification of PR3, PR4, and SAR3.

2) Method

A styrofoam head and plastic eye-shaped sphere were used to verify whether the prototypes worked in conjunction with the PSS. First, the PI was placed onto the plastic sphere according to the 20-degree rotation (PR3) using the RCMP. To test the RoM (PR4), the IM was moved from the lower to the upper limit of the Ψ and Φ DoFs. Moving I and Θ was not required. Finally, the quick release of the IM was initiated (SAR3). Recordings were made of these steps, and an image of the setup is presented in Figure 14.

3) Results Both PIs could be placed within the surgical field defined by the styrofoam head and plastic sphere. The IMF-connector achieved the 20-degree rotation. However, for the IMS-connector, the styrofoam had to be rotated towards the IM.

Both connectors limited the RoM of the PSS. Mainly, the Φ DoF was restricted, which can be seen in the supplemented RoM video's.

The IM was quick-releasable for all connectors and PIs, therefore. The IMS-connector and the PI stayed in their place during IM retraction. The IMF-connector, PI, and IM were quickly releasable within 2 seconds (supplemented retraction video).

4) Discussion Both PIs could be placed in the surgical field with the IMF-connector, by which PR3 is met even though fixed dimensions are used for the styrofoam head and plastic eye. Since the RCMP is designed to adjust the RCM to different eyes and patients, the placement and rotation of the PI will be achieved on a variety of eyes as well.

The IMS-connector would require a design iteration because the IMS-connector obstructed translation in the X direction

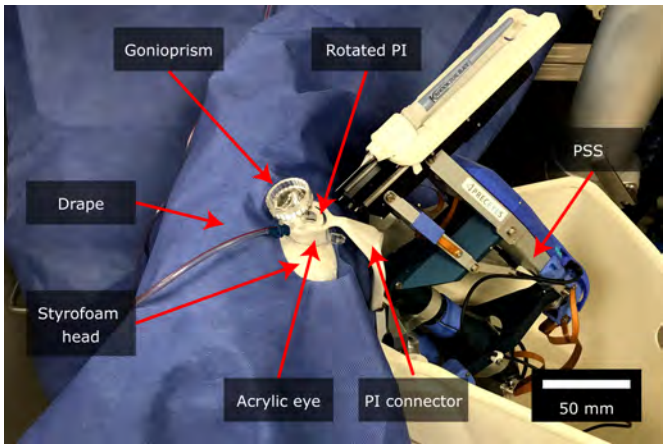

Fig. 14: Setup bench test (scale is indicative)

due to the material between the HR and the IMS. A future design should have less material between the HR and IMS, or the PI should be connected elsewhere to the IMS.

The RoM of the IM was initially limited due to protruding bolts at the IMH that coincided with the thickened ribs, which was partly solved by removing some of the material, providing more RoM for the IM. These interfaces would require a design iteration but will be sufficient to meet PR4 as presented in subsection IV-E

The IM was quick-releasable within two seconds, by which SAR3 is also met. It is demonstrated without an SI inserted in the eye and without the PI sucked onto the (plastic) eye. Nevertheless, SAR3 is met as long as the PIs meet SAR4. Because then the retraction of the SI will not be affected by the connectors or PIs and the retraction of the SI and IM is within 2 seconds by definition. Furthermore, the retraction of the PI starts with a translation in the X direction, which could potentially harm the eye and should be investigated further.

E. KDB procedure experiment

An anterior segment procedure was performed on an ex-vivo eye with the Kahook Dual Blade (KDB).

1) Purpose

The purpose of the experiment was the verification of PR1, PR2, PR4 and SAR4.

2) Method

An acrylic setup was used to position the porcine eye holder with the porcine eye within normal reach of the IM. Furthermore, a KDB was used and clamped to the IM head. The setup is shown in Figure 15. Since ex vivo porcine eyes were used in the setup, draping provided a sterile barrier.

As preparation for this experiment, the surgical system, microscope, setup and draping are all installed. Hereafter the experiment is done according to the following procedure:

1) Prepare porcine eye and place it with the porcine eye holder in the acrylic setup.
2) Make a corneal incision with the surgical blade at the limbus.
3) Place suction PI with suction pressure of 300 mbar (SAR2).
4) Inflate anterior chamber with viscoelastic (Viscoat, Alcon).
5) Place viscoelastic on the cornea and position gonioprism to visualise the trabecular meshwork (TM) (PR2).
6) Insert the KDB through the incision point (PR1).
7) Settle the footplate of the KDB on the anterior wall of Schlemm's canal. Open up the TM by making an incision in the inner wall.
8) Swiping motion over an arc of 60 degrees to remove the inner wall in the clockwise direction. Flip the instrument 180 degrees and swipe 60 degrees in the counterclockwise direction (PR4).
9) Retract instrument and remove suction tube to verify quick-releasibility of the PI (SAR4).

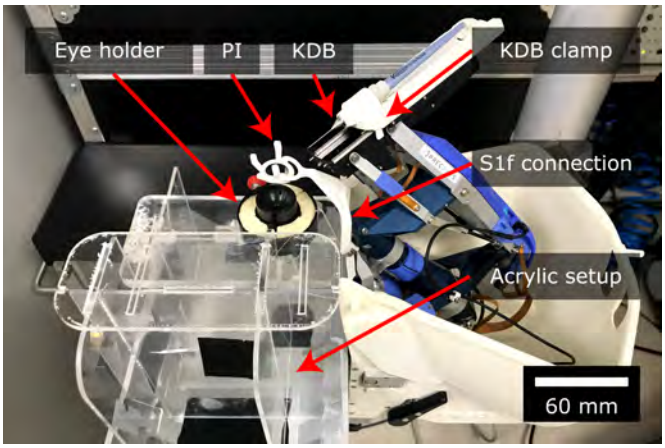

Fig. 15: Setup ex vivo KDB experiment (scale is indicative)

3) Results

Two eyes were used for the KDB procedure. All procedure steps were successfully performed (presented in supplemented KDB video).

PI was placed on the eye and held the eye robustly for a prolonged time. The eye could be lifted out of the porcine eye holder, indicating a suction force is applied of at least 275 mN (based on the mass of a human eye). Insertion of a SI was achieved by inserting the KDB into the eye, and visualisation of the angle structure was achieved. However, other gonio equipment was used than the Volk gonioprism.

The swiping motions were performed without using the gonioprism and could be made in both directions, reaching 180 degrees of the TM.

Finally, both PIs could be released within two seconds by removing the suction tube of the PI.

4) Discussion

To allow the KDB to be inserted in the eye by which PR1 is met, the incision had to be expanded. Because the alignment of the incision point and RCM is difficult. In the experiment, first, the incision was made, and then the PI was placed, making the alignment complex, especially for the O-PI, which has material at both sides of the joint.

The SI could reach at least 120 degrees of the TM during tissue manipulation, which was needed for the Ψ DoF. Reaching the TM is the lowest angle needed for the Φ DoF. Because the PI and connector enabled this lower angle and higher angles are not obstructed, the RoM is considered sufficient to perform anterior segment surgery, by which PR4 is met.

SAR4 is met since the PIs were released within two seconds, although it was verified by manually removing the suction tube. Ideally, releasing the PI will be implemented in the quick-releasable workflow of the PSS.

Clear visualisation of the angle structure was verified using a microscope and a gonioprism, by which PR2 was met. Although, it was verified using a handheld gonioprism, which could not be docked onto the PIs. Furthermore, the PI's inner diameter was too small, causing the PI to overlap the cornea slightly. Due to the porcine eye not having a circular shape but an oval-shaped cornea with a longer length than

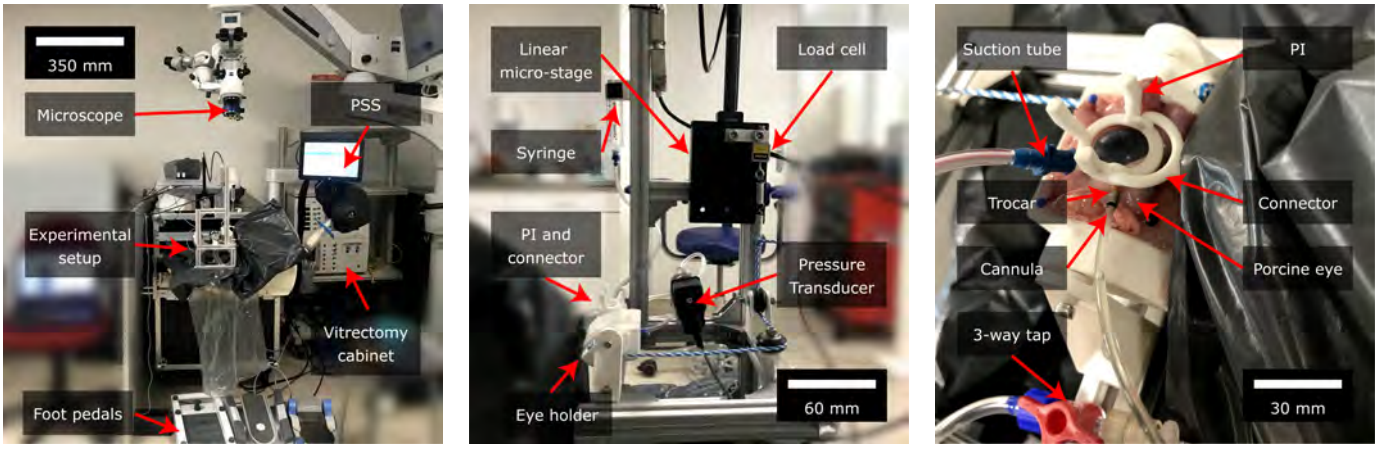

(a) Global setup (b) Experimental setup (c) Eye holder setup

Fig. 16: Experimental setup ex vivo performance measurement (scale is indicative)

a human corneal diameter. Consequently, visualisation of the angle structure and tissue manipulation was complex. A future design should have a larger inner diameter to better fit better onto porcine eyes.

The results in the experiment are not affected by the type of connector used. Due to the opaque of the porcine eyes, only the IMF prototype was verified. Furthermore, Each step can be done individually, although the workflow of the procedure was not tested as a whole. The procedure was not done by a surgeon and without a time limit.

F. Performance experiment

An ex-vivo experiment is done to determine the performance of the PI and connector prototypes.

1) Purpose

The purpose of the experiment is the verification of the SSR1, SSR2, SSR3, SAR1, and SAR2.

2) Method

The setup used to measure the BAF, IOP, and accuracy is similar to the setup presented in subsection III-D. Modifications are made to allow video recording with the microscope and fit the setup into the headrest (Figure 16a). The eye holder is designed to enable placement of the connector, PI, and foam (Figure 16c). The eyes used were stored for one or two days in the refrigerator. Furthermore, a spring is placed between the load cell, and the pull rope (Figure 16b) and aluminium connectors are used to connect the transducer to the tubing. The procedure that is followed is also similar to the comparison experiment:

1) Prepare the porcine eye and pin it down to the eye holder Figure 16c
2) Insert the porcine intravitreal with a trocar in the pars plana at 4 mm of the limbus in the direction of the centre of the globe. Hereafter, insert the cannula in the trocar and set IOP at 15 mmHg using the height-adjustable syringe (Figure 16b).
3) Dock PI onto the eye and apply a suction pressure of 300 mbar using the vitrectomy cabinet. Consequently, SAR2 will be met, and the IOP will rise (SAR1). To minimise the effect of compression on the eye, the translations in X, Y, and Z are adjusted such that the rise in IOP is minimal.
4) Rotate the eye by translating the RCMP 1.4 mm and 4 mm in the anterior and medial directions, respectively (SSR1). Hereafter, bring the eye back to its original position.
5) Start recording with the microscope and set displacement of linear micro-stage to exert a pull force to the eye.
6) When the eye breaks away, the BAF and IOP are noted, the video is stopped, and the displacement is reset (SSR2, SSR3, and SAR1).

The measurement data obtained was processed such that the moment of breakaway took place at 8 seconds by translating the data over the x-axis. Hereafter, the mean and 95 % confidence interval was calculated and plotted.

3) Results

Intravitreal insertion of the trocar was complex due to the suction ring. Initially, experiments were done on eight eyes in total (four for each connector). However, due to placement issues of the trocar, the IOP could only be successfully measured in two eyes. To ensure these results were significant, multiple tests were done on these eyes. Four sets of measurements were obtained for the U-PI IMS-connector combination ($N=4$) and three sets for the other combinations ($N=3$), as shown in appendix C.

Both the IMF- and IMS-connectors were able to rotate the PIs up to 20 degrees using the RCMP of the PSS.

The BAF and IOP were measured successfully on one eye for both connectors (Figure 17). The micro-stage pulled the eye, and consequently, the eye rotated and broke away (as can be seen in supplemented break away videos).

The mean IOP stayed below 30 mmHg and 25 mmHg for the O-PI and U-PI, respectively. The 95% interval also stayed well within limits. The difference between the mean IOPs of the two connectors was less than 2.5 mmHg.

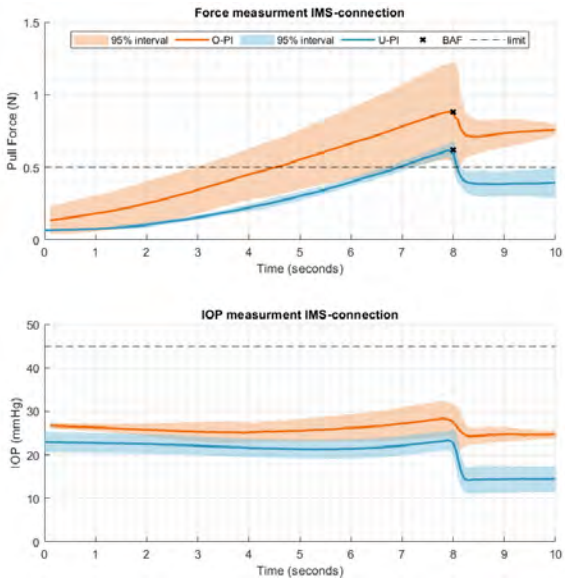

(a) IMS-connector

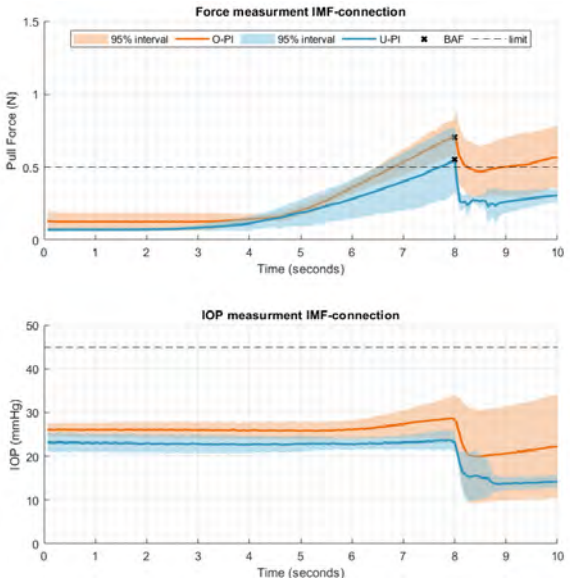

(b) IMF-connector

Fig. 17: Force and IOP measurements during eye pulling. Breakaway is set at 8 seconds.

The mean BAFs were above the lower limit of 500 mN for all connectors and PIs. The mean BAFs for the IMF connector were 707 mN and 551 mN for the O-PI and U-PI, respectively. The mean BAFs for the IMs-connector were 881 mN and 618 mN for the O-PI and U-PI, respectively. The 95% confidence interval of the IMF-connector combined with the U-PI did not stay above the limit of 500 mN. The 95% confidence interval of the other interfaces all stayed above the limit of 500 mN.

Finally, the fixation accuracy was determined by comparing a capture before rotation with capture just before the breakaway. The videos used to select the captures were made with the microscope in the setup and are supplemented to this study. Due to the resolution of the footage used, the accuracy cannot be determined up to 25 µm. Six colour image tracing is used to cluster and curve pixels, which allowed magnification of the microscopic recordings and resulted in the figures presented in Figure 18. The displacement of the limbus of the IMF- and IMS-connector are estimated at 150 µm and 50 µm, respectively.

4) Discussion The eyes could be rotated 20 degrees for combinations of all PIs and connectors by which SSR1 is met. When alignment was acquired, the rotation could be achieved by X and Z translation. However, the alignment of PI and eye was a challenge, similar to what was encountered in the kahook dual procedure experiment.

Despite differences between connectors and PIs, the mean BAF for all combinations were more than the lower limit of 500 mN, by which SSR2 is met. A difference in alignment or compression could explain the difference in BAF between the two connectors. Furthermore, different eyes were used for each connector. The program and settings were reset in-between the measurements, which led to different settings between the connectors and thus different slopes of the pull force.

The difference in BAF between the PIs (the U-PI is 70-80 % compared with the O-PI) can be explained by the difference in the suction area, which (the U-PI is 63 % compared with the O-PI). A lower suction area means a lower suction force and thus a lower BAF. Furthermore, the U-PI can rotate around the hinge, whereas this rotation is constrained for O-PI. To compensate for the difference in BAF, the P_S for the U-PI should be increased, ensuring the 95% confidence interval stays above the limit.

The difference in the BAF values presented here and the BAF values presented in subsection III-D is due to different design parameters in the comparison experiment: the initial IOP was 20 mmHg, the IOP was increased to 50 mmHg, the P_S was 320 mbar, the F_C was 296 mN, and the suction area was 214 mm^2. In the experiment presented here, the initial IOP was 15 mmHg, the IOP was increased to 24-28 mmHg, the P_S was 300 mbar, the F_C is unknown, and the suction areas were 104 and 166 mm^2. Furthermore, the PI was connected to linear rail, and in the experiment presented here, the PI has is hinged and connected to the PSS. These differences cause the BAF to be lower, but it is unknown to what amount each parameter plays a role.

The mean IOP stayed below the upper limit of 45 for both connectors and PIs by which SAR1 is met. The difference in the suction area explains the difference between the PIs. Less suction area means less deformation of the sclera and thus less increase in IOP. The rise in IOP values of the U-PI is 60-65 % compared with the O-PI, and the suction area of the U-PI is 63 % compared with the O-PI.

The rise in IOP is less than a factor 0.5 with respect to the values presented in subsection III-D, which can be explained by the lower P_S, suction area and compression force. Furthermore, a decrease in IOP can be observed in both

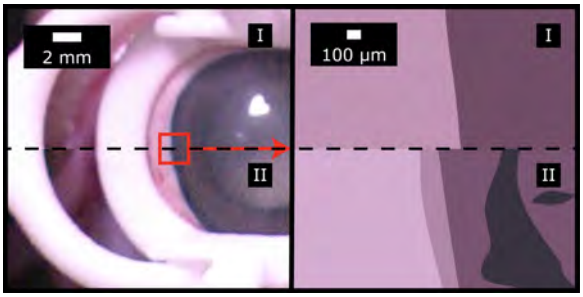

(a) IMF-connector with O-PI

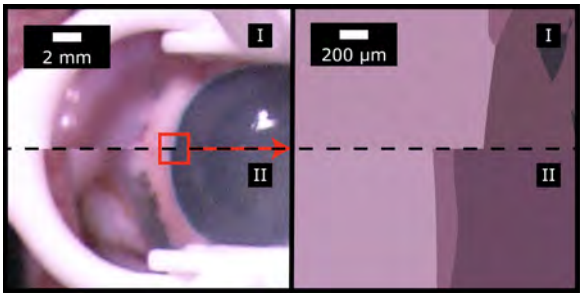

(b) IMF-connector with U-PI

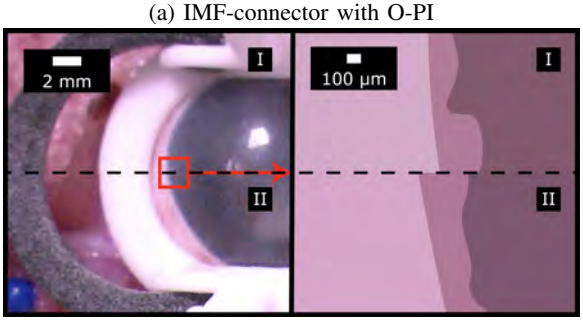

(c) IMS-connector with O-PI

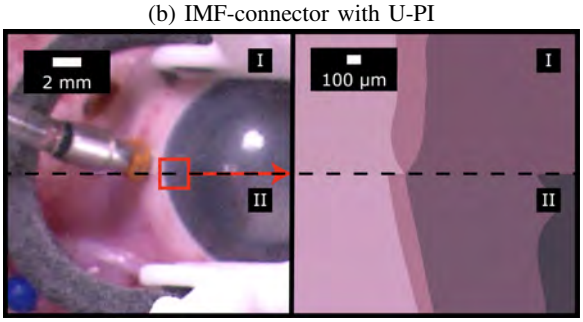

(d) IMS-connector with U-PI

Fig. 18: Configuration I. before rotation and II. before breakaway

experiments, even though aluminium connectors were used for the transducer.

The displacement due to the BAF was estimated at 50 and 150 µm for the IMS- and IMF-connectors, respectively. The accuracy found could have been affected by vibrations of the microscope and deflection of the connector itself. Although this accuracy exceeds the limit of 25 µm, SSR3 can neither be met nor rejected. Since this displacement is a consequence of the connector deflections due to the pull force exerted. The DoFs of the IM can compensate for this displacement. Therefore, the displacement shown here does not limit the potential of the robotic system. The accuracy should be measured during stable docking and constant muscle force while manipulating tissue inside the eye.

V. General discussion

To summarise, this study presents the design characteristics of an interface that mechanically fixates and stabilises the eye to perform robotic-assisted surgery in the anterior segment. First, an investigation into three fixation concepts (friction, suction, and insertion) and associated limits for (in)dependent variables. Three prototypes are designed, and their ability to stabilise the eye is experimentally compared, in which suction performs best. Hereafter, two suction interfaces and two connectors are successfully designed and manufactured according to safe limits and drafted requirements for this integration. The O-PI combined with the IMF-connector performed best. However, if the P_S is increased for the U-P, it will have a similar performance. The IMS will need significant design changes before it can be used in conjunction with the PSS. All in all, both PIs in combination with IMF-connector enable anterior segment surgery by the Preceyes surgical system, stabilises the eye, and allow insertion of a SI into the eye.

Since the discussions of each experiment are already presented, the general discussion will consist of a discussion of the requirements followed by recommendations for future research and future designs.

The limit for the eye rotation up to 20-degree eye should be set less strict (SSR1). The limit set was based on the results of an ex-vivo KDB experiment and was estimated to be 20 degrees at most. This limit was primarily used in the detailed design section and did affect the design of the PIs. The angle at which this interface and connector are designed will enable the PSS to perform an anterior segment procedure. However, a limit of 10-15 degrees may be sufficient as well.

The limit set in this for the rise in IOP should be made more strict (SAR1). The limit is based on perfusion pressure. This limit may be decreased to ensure a safe surgical procedure, especially if glaucomatous eyes are used in such a procedure, which already have an elevated IOP ($\geq$ 22 mmHg). Setting a lower limit can be done without adjusting to the design since the IOP stayed well under the IOP limit for the presented interfaces.

Additionally, the requirement for the holding force is chosen at an upper limit multiplied by a safety factor of two. If the upper limit for the rotation is decreased, the limit for the holding force will be up to three times more than the force necessary for eye fixation. However, only one eye muscle has been considered in this limit, so if two muscles are exerted simultaneously, the muscle force could be higher. On the other hand, an F_C of only 178 mN was considered sufficient for eye fixation [32]. Although the limit of 500 may have been set too strict, it guarantees safe eye stabilisation.

A. Recommendations for future research

It is recommended to evaluate other concepts further, where they were not developed (in detail). For example, the insertion prototype could be improved significantly, potentially leading to more promising results. Furthermore, wet adhesion using micro-patterns could become a suitable fixation concept. The forces these microstructures currently can generate are not yet sufficient for eye fixation. However, a considerable amount of research is being done in this field [59]. Furthermore, other connector concepts could be investigated. For example, concepts could be developed where the PI is connected to a speculum, the IMH or the HR.

Further research should provide more insight into the relationships of compression forces, suction pressures, contact or suction areas, and IOP. Finding the optimal P_S and F_C is crucial to guarantee a tolerable IOP and sufficient stability for a safe surgical procedure. Furthermore, further research should be done if the loss in IOP affects eye stabilisation. If so, the IOP could be increased by, for example, 5 mbar per minute [53].

An additional experiment should be done to verify the accuracy (SSR3) and angle structure visualisation (PR2) during tissue manipulation. Ideally, in a procedure performed by an experienced surgeon. In this experiment, the suction pressure and compression force could be measured with sensory equipment since the actual value is regulated only.

To validate a further developed design, the performance should be better identified with more measurements, taking variation into account. In the experiment, attention should be paid to artificial lubrication, which has been out of scope in this research. Furthermore, a two DoF test setup could be used or be used. Alternatively, the experiment could also be done in-vivo since this is the most realistic setting. A clinical trial could be needed in later stages before bringing a final design to the market, depending on the risk assessment and classification.

Finally, it is recommended to research the side effects of eye stabilisation on in-vivo eyes. This study focused on the safe limits for interfaces used for eye stabilisation and their mechanical performance. Inflammation, patient discomfort, or IOP recovery was considered out of scope. In the short and long term, inflammation and IOP recovery could play a role, which should be researched. In some of the ex-vivo measurements, slight inflammation (red spots) have been observed. However, it is unknown if the suction interface caused these red spots.

B. Recommendations for future designs

It is recommended that a future design meets medical regulations, e.g. medical electrical equipment (IEC 60601-1), which leads to additional requirements. Components coming into contact with the patient shall be made either disposable or sterilisable, bio-compatible materials shall be used where materials come into contact with the patient, and the system shall have a single fault safe design. Satisfaction with these regulations is already achieved or could be achieved easily. The PIs are disposable and are made of a biocompatible material. Furthermore, risk assessments should be done to research the single-fault safe characteristic. Risks that should be assessed are, for example, the loss of suction and quick-release of the PI. Another opportunity to improve the PI design is implementing a chamber filled with viscoelastic fluid to maintain eyeball hydration and persevering an unobstructed path for optical instruments during intraocular surgical procedures [60].

Improvements should also be made in the design of the connectors. The creation of a sterile barrier should be implemented in the design of both the connector and draping. For example, the design could be made out of two parts containing a snap-fit connection. Another design possibility is the joint connection with the PI. The hinge could be made compliant, or stable passive docking could be achieved by using the torsional spring property of the eye. Passive docking will simplify the docking of the PI onto the eye and could potentially simplify the alignment. Research should be done into the consequences for the accuracy of these alternative concepts.

It is recommended to improve the integration of the PI and connector with the PSS. The suction pressure should be regulated within the software of the PSS. This should also enable quick retraction of the PI within the quick releasable workflow of the IM. The retraction of the PI could be made faster by quickly generating a puff of air. Secondly, real-time measurements of the IOP or P_S would make it possible to notice a loss in suction pressure, which could initiate the retraction protocol. The measured and regulated values could be implemented in the user interface of the PSS. Finally, placement, alignment and rotation of the PI could be implemented in the software. Ideally, the eye is first docked, then the incision is made with an instrument held by the IMH to ensure alignment with the RCM. Hereafter, the rotation around the Eye's CoR could be initiated, programmed in the software.

VI. Conclusion

This work reported on the development of an interface that mechanically fixates and stabilises the eye. Three concepts to stabilise the eye are introduced: friction, suction, and insertion and compared in an ex-vivo experiment. All interfaces were set up with a rise in IOP of approximately 30 mmHg by regulating the compression force and suction pressure. Consequently, the force was measured needed to pull the eye such that it broke away. The BAF needed for the suction interface was 5 and 2.7 times higher than the insertion and friction interfaces, respectively. Therefore, suction was considered most suited for eye stabilisation.

Suction was further developed in a U-PI and O-PI. Furthermore, two connectors are designed to connect the interface to the surgical system. A bench test demonstrated that the IMF is most suited for integration in the surgical system, and the IMS needs a design iteration. An experiment is performed on an ex-vivo porcine eye to demonstrate that a KDB procedure could be performed. All procedural steps were verified. However, further development is needed to better identify the accuracy

and visualise the angle structure during tissue manipulation. In a third experiment, the performance was identified. For both connectors, the mean rise IOP of the U-PI and O-PI stayed below 10 and 15 mmHg, respectively. The mean BAF for all PIs and connectors were above the lower limit of 500 mN.

To conclude, in this study, a proof of concept is presented for a design of an interface that mechanically fixates and stabilises the eye to perform anterior segment surgery by the Preceyes surgical system. Both PIs combined with the IMF-connector stabilised the eye with sufficient holding force while keeping the IOP within safe limits. Furthermore, placement in the surgical field, SI insertion, angle structure visualisation, and eye rotation was enabled.

Acknowledgements

The author wishes to thank Preceyes B.V. for funding this work, Dr Marc de Smet for a helpful discussion and Harmen aan het Rot, Sebastiaan Schipper and Stijn van der Ploeg for proofreading this article. He also thanks Mr Jos van Driel for his excellent technical assistance.

References

[1] R. R. A. Bourne, J. Adelson, S. Flaxman, P. Briant, M. Bottone, T. Vos, K. Naidoo, T. Braithwaite, M. Cicinelli, J. Jonas, H. Limburg, S. Resnikoff, A. Silvester, V. Nangia, and H. R. Taylor, "Global Prevalence of Blindness and Distance and Near Vision Impairment in 2020: progress towards the Vision 2020 targets and what the future holds." *Investigative Ophthalmology & Visual Science*, vol. 61, no. 7, pp. 2317–2317, Jun. 2020. [Online]. Available: https://iovs.arvojournals.org/article.aspx?articleid=2767477

[2] E. Abedloo, S. Gholami, and H. D. Taghirad, "Eye-RHAS manipulator: From kinematics to trajectory control," *International Conference on Robotics and Mechatronics*, pp. 61–66, 2015. [Online]. Available: https://ieeexplore.ieee.org/document/7367761

[3] M. J. Gerber, M. Pettenkofer, and J.-P. Hubschman, "Advanced robotic surgical systems in ophthalmology," *Eye (Basingstoke)*, vol. 34, no. 9, pp. 1554–1562, 2020. [Online]. Available: https://www.nature.com/articles/s41433-020-0837-9

[4] R. Nuzzi and L. Brusasco, "State of the art of robotic surgery related to vision: Brain and eye applications of newly available devices," *Eye and Brain*, vol. 10, pp. 13–24, 2018. [Online]. Available: https://www.ncbi.nlm.nih.gov/pmc/articles/PMC5798758/

[5] H. B. Dick and T. Schultz, "A Review of Laser-Assisted Versus Traditional Phacoemulsification Cataract Surgery," *Ophthalmology and Therapy*, vol. 6, no. 1, pp. 7–18, Jun. 2017. [Online]. Available: https://www.ncbi.nlm.nih.gov/pmc/articles/PMC5449299/

[6] R. Heitel and H. Fu, "Systems and methods for dynamic patient fixation system," US Patent US20 140 218 689A1, Aug., 2014. [Online]. Available: https://patents.google.com/patent/US20140218689A1/en?oq=US+2014%2f0218689+A1+

[7] M. Gertner, M. Arnoldussen, and M. Herron, "Device and assembly for positioning, stabilizing and treating an eye," EP Patent EP2 152 142B1, Jul., 2013. [Online]. Available: https://patents.google.com/patent/EP2152142B1/en?oq=EP2152142B1

[8] B. C. Becker and C. N. Riviere, "Real-time retinal vessel mapping and localization for intraocular surgery," *IEEE Int Conf Robot Autom*, pp. 5360–5365, 2013. [Online]. Available: https://ieeexplore.ieee.org/document/6631345

[9] B. C. Becker, R. A. Maclachlan, L. A. J. Lobes, G. D. Hager, and C. N. Riviere, "Vision-Based Control of a Handheld Surgical Micromanipulator with Virtual Fixtures." *IEEE transactions on robotics : a publication of the IEEE Robotics and Automation Society*, vol. 29, no. 3, pp. 674–683, 2013.

[10] M. D. De Smet, G. J. L. Naus, K. Faridpooya, and M. Mura, "Robotic-assisted surgery in ophthalmology," *Current Opinion in Ophthalmology*, vol. 29, no. 3, pp. 248–253, 2018.

[11] "Preceyes BV – High-precision assistance for eye surgery." [Online]. Available: http://www.preceyes.nl/

[12] D. A. L. Maberley, M. Beelen, J. Smit, T. Meenink, G. Naus, C. Wagner, and M. D. de Smet, "A comparison of robotic and manual surgery for internal limiting membrane peeling," *Graefe's Archive for Clinical and Experimental Ophthalmology*, vol. 258, no. 4, pp. 773–778, 2020.

[13] T. Bourcier, M. Nardin, A. Sauer, D. Gaucher, C. Speeg, D. Mutter, J. Marescaux, and P. Liverneaux, "Robot-Assisted Pterygium Surgery: Feasibility Study in a Nonliving Porcine Model." *Translational vision science & technology*, vol. 4, no. 1, p. 9, 2015.

[14] D. A. Belyea, M. J. Mines, W.-J. J. Yao, J. A. Dan, and K. S. Bower, "Telerobotic contact transscleral cyclophotocoagulation of the ciliary body with the diode laser," *Journal of Robotic Surgery*, vol. 8, no. 1, pp. 49–55, 2014.

[15] R. Webb, M. Brownell, C. Horvath, T. Juhasz, R. Kurtz, L. Nagy, M. Ross, and C. Suarez, "Ocular fixation and stabilization device for ophthalmic surgical applications," US Patent US20 040 225 284A1, Nov., 2004. [Online]. Available: https://patents.google.com/patent/US20040225284A1/en?oq=US20040225284A1

[16] M. D. de Smet, T. C. M. Meenink, T. Janssens, V. Vanheukelom, G. J. L. Naus, M. J. Beelen, C. Meers, B. Jonckx, and J.-M. Stassen, "Robotic Assisted Cannulation of Occluded Retinal Veins," *PLOS ONE*, vol. 11, no. 9, p. e0162037, Sep. 2016. [Online]. Available: https://dx.plos.org/10.1371/journal.pone.0162037

[17] I. Kozak and U. Rahn, "Navigation technology/eye-tracking in ophthalmology: principles, applications and benefits—a narrative review," *Annals of Eye Science*, vol. 6, no. 0, pp. 6–6, Mar. 2021. [Online]. Available: https://aes.amegroups.com/article/view/5776

[18] J. T. Wilson, M. J. Gerber, S. W. Prince, C. W. Chen, S. D. Schwartz, J. P. Hubschman, and T. C. Tsao, "Intraocular robotic interventional surgical system (IRISS): Mechanical design, evaluation, and master–slave manipulation," *International Journal of Medical Robotics and Computer Assisted Surgery*, vol. 14, no. 1, 2018. [Online]. Available: https://pubmed.ncbi.nlm.nih.gov/28762253/

[19] V. Kadambi and F. Tang, "Active eye movement and positioning control device," US Patent US5 947 955A, Sep., 1999. [Online]. Available: https://patents.google.com/patent/US5947955A/en?oq=US5947955A

[20] C. Power, C. Crowe, P. Higgins, and D. C. Moriarty, "Anaesthetic depth at inductionAn evaluation using clinical eye signs and EEG polysomnography," *Anaesthesia*, vol. 53, no. 8, pp. 736–743, 1998. [Online]. Available: https://associationofanaesthetists-publications.onlinelibrary.wiley.com/doi/abs/10.1046/j.1365-2044.1998.00468.x

[21] J. S. Pannu, "Device and method for stabilization of eye during eye surgery," US Patent US20 080 147 149A1, Jun., 2008. [Online]. Available: https://patents.google.com/patent/US20080147149A1/en?oq=US20080147149A1

[22] J. H. Talamo, P. Gooding, D. Angeley, W. W. Culbertson, G. Schuele, D. Andersen, G. Marcellino, E. Essock-Burns, J. Batlle, R. Feliz, N. J. Friedman, and D. Palanker, "Optical patient interface in femtosecond laser–assisted cataract surgery: Contact corneal applanation versus liquid immersion," *Journal of Cataract and Refractive Surgery*, vol. 39, no. 4, pp. 501–510, Apr. 2013. [Online]. Available: https://journals.lww.com/02158034-201304000-00004

[23] C. Strohmaier, C. Runge, O. Seyeddain, M. Emesz, C. Nischler, A. Dexl, G. Grabner, and H. A. Reitsamer, "Profiles of Intraocular Pressure in Human Donor Eyes during Femtosecond Laser Procedures—A Comparative Study," *Investigative Opthalmology & Visual Science*, vol. 54, no. 1, p. 522, Jan. 2013. [Online]. Available: http://iovs.arvojournals.org/article.aspx?doi=10.1167/iovs.12-11155

[24] A. Ebrahimi, C. He, M. Roizenblatt, N. Patel, S. Sefati, P. Gehlbach, and I. Iordachita, "Real-Time Sclera Force Feedback for Enabling Safe Robot-Assisted Vitreoretinal Surgery," in *2018 40th Annual International Conference of the IEEE Engineering in Medicine and Biology Society (EMBC)*. Honolulu, HI: IEEE, Jul. 2018, pp. 3650–3655. [Online]. Available: https://ieeexplore.ieee.org/document/8513255/

[25] "Understanding Aqueous Humor and Vitreous Humor (The Differences)." [Online]. Available: https://www.nvisioncenters.com/education/aqueous-and-vitreous/

[26] "Human Eye Anatomy - Parts of the Eye Explained." [Online]. Available: https://www.allaboutvision.com/resources/anatomy.htm

[27] "SMART - Servier Medical ART." [Online]. Available: https://smart.servier.com/

[28] "Eye Pressure," Jan. 2018. [Online]. Available: https://www.aao.org/eye-health/anatomy/eye-pressure

[29] J. Flammer and M. Mozaffarieh, "The Mechanism of Glaucomatous Damage to the Optic Nerve," *European Ophthalmic Review*, Mar. 2011. [Online]. Available: https://www.touchophthalmology.com/glaucoma/journal-articles/the-mechanism-of-glaucomatous-damage-to-the-optic-nerve/

[30] M. D. de Smet, J. M. Stassen, T. C. M. Meenink, T. Janssens, V. Vanheukelom, G. J. L. Naus, M. J. Beelen, and B. Jonckx, "Release of experimental retinal vein occlusions by direct intraluminal injection of ocriplasmin," *The British Journal of Ophthalmology*, vol. 100, no. 12, pp. 1742–1746, Dec. 2016. [Online]. Available: https://www.ncbi.nlm.nih.gov/pmc/articles/PMC5256413/

[31] O. Sterner, C. Karageorgaki, M. Zürcher, S. Zürcher, C. W. Scales, Z. Fadli, N. D. Spencer, and S. G. P. Tosatti, "Reducing Friction in the Eye: A Comparative Study of Lubrication by Surface-Anchored Synthetic and Natural Ocular Mucin Analogues," *ACS Applied Materials & Interfaces*, vol. 9, no. 23, pp. 20 150–20 160, Jun. 2017. [Online]. Available: https://doi.org/10.1021/acsami.6b16425

[32] S. Russo, G. Petroni, C. Quaglia, M. Niccolini, F. Rossi, L. Menabuoni, R. Pini, D. Fortuna, P. Dario, and A. Menciassi, "ESPRESSO: A novel device for laser-assisted surgery of the anterior eye segment," *Minimally Invasive Therapy and Allied Technologies*, vol. 25, no. 2, pp. 70–78, 2016.

[33] J. Colter, B. Wirostko, and B. Coats, "Coefficient of friction between Carboxymethylated Hyaluronic acid-based polymer films and the ocular surface," *Investigative Ophthalmology and Visual Science*, vol. 58, no. 14, pp. 6166–6174, Dec. 2017.

[34] S. Mariacher, M. Mariacher, A. M. Seuthe, P. Szurman, B. Seitz, and K. T. Boden, "Impact of Patient Interface Diameter and Vacuum Level on Suction Stability Using a Flat Applanating Interface for Femtosecond Laser-Assisted LASIK," *Current Eye Research*, vol. 45, no. 7, pp. 789–796, Jul. 2020. [Online]. Available: https://www.tandfonline.com/doi/full/10.1080/02713683.2019.1701688

[35] J. Koelling, "Microkeratome," Aug. 2014. [Online]. Available: https://www.aao.org/image/microkeratome

[36] I. Sánchez, R. Martin, F. Ussa, and I. Fernandez-Bueno, "The parameters of the porcine eyeball," *Graefe's archive for clinical and experimental ophthalmology = Albrecht von Graefes Archiv für klinische und experimentelle Ophthalmologie*, vol. 249, pp. 475–82, Feb. 2011.

[37] M. W. Charles and N. Brown, "Dimensions of the human eye relevant to radiation protection," *Physics in Medicine and Biology*, vol. 20, no. 2, pp. 202–218, Mar. 1975.

[38] Z. He, B. V. Bui, and A. J. Vingrys, "The Rate of Functional Recovery from Acute IOP Elevation," *Investigative Ophthalmology & Visual Science*, vol. 47, no. 11, pp. 4872–4880, Nov. 2006. [Online]. Available: https://iovs.arvojournals.org/article.aspx?articleid=2125641

[39] E. Stefánsson, D. B. Pedersen, P. K. Jensen, M. la Cour, J. F. Kiilgaard, K. Bang, and T. Eysteinsson, "Optic nerve oxygenation," *Progress in Retinal and Eye Research*, vol. 24, no. 3, pp. 307–332, May 2005. [Online]. Available: https://linkinghub.elsevier.com/retrieve/pii/S1350946204000801

[40] K. V. Keer, J. B. Breda, L. A. Pinto, I. Stalmans, and E. Vandewalle, "Estimating Mean Ocular Perfusion Pressure Using Mean Arterial Pressure and Intraocular Pressure," *Investigative Ophthalmology & Visual Science*, vol. 57, no. 4, pp. 2260–2260, Apr. 2016. [Online]. Available: https://iovs.arvojournals.org/article.aspx?articleid=2519757

[41] R. L. Radius and D. R. Anderson, "Reversibility of optic nerve damage in primate eyes subjected to intraocular pressure above systolic blood pressure." *British Journal of Ophthalmology*, vol. 65, no. 10, pp. 661–672, Oct. 1981. [Online]. Available: https://bjo.bmj.com/lookup/doi/10.1136/bjo.65.10.661

[42] C. Balaratnasingam, W. H. Morgan, L. Bass, G. Matich, S. J. Cringle, and D.-Y. Yu, "Axonal Transport and Cytoskeletal Changes in the Laminar Regions after Elevated Intraocular Pressure," *Investigative Opthalmology & Visual Science*, vol. 48, no. 8, p. 3632, Aug. 2007. [Online]. Available: http://iovs.arvojournals.org/article.aspx?doi=10.1167/iovs.06-1002

[43] C. Balaratnasingam, W. H. Morgan, L. Bass, S. J. Cringle, and D.-Y. Yu, "Time-Dependent Effects of Elevated Intraocular Pressure on Optic Nerve Head Axonal Transport and Cytoskeleton Proteins," *Investigative Ophthalmology & Visual Science*, vol. 49, no. 3, pp. 986–999, Mar. 2008. [Online]. Available: https://iovs.arvojournals.org/article.aspx?articleid=2184509

[44] M. Ebner, S. Mariacher, K. Januschowski, K. Boden, A.-M. Seuthe, P. Szurman, and K. T. Boden, "Comparison of intraocular pressure during the application of a liquid patient interface (FEMTO LDV Z8) for femtosecond laser-assisted cataract surgery using two different vacuum levels," *British Journal of Ophthalmology*, vol. 101, no. 8, pp. 1138–1142, Aug. 2017. [Online]. Available: https://bjo.bmj.com/content/101/8/1138

[45] G. P. Williams, H. P. Ang, B. L. George, Y. C. Liu, G. Peh, L. Izquierdo, D. T. Tan, and J. S. Mehta, "Comparison of intra-ocular pressure changes with liquid or flat applanation interfaces in a femtosecond laser platform," *Scientific Reports*, vol. 5, no. 1, p. 14742, Dec. 2015. [Online]. Available: http://www.nature.com/articles/srep14742

[46] K. T. Boden, M. Mariacher, K. Januschowski, K. Boden, A. Rickmann, P. Szurman, B. Seitz, and S. Mariacher, "Stability of a non-applanating handheld liquid patient interface for femtosecond laser-assisted cataract surgery," *International Ophthalmology*, vol. 40, no. 10, pp. 2683–2689, Oct. 2020. [Online]. Available: http://link.springer.com/10.1007/s10792-020-01450-0

[47] A. K. Golahmadi, D. Z. Khan, G. P. Mylonas, and H. J. Marcus, "Tool-tissue forces in surgery: A systematic review," *Annals of Medicine and Surgery*, vol. 65, p. 102268, May 2021. [Online]. Available: https://www.sciencedirect.com/science/article/pii/S2049080121002181

[48] D. A. Robinson, D. M. O'Meara, A. B. Scott, and C. C. Collins, "Mechanical components of human eye movements," *Journal of Applied Physiology*, 1969.

[49] S. Schutte, S. P. W. van den Bedem, F. van Keulen, F. C. T. van der Helm, and H. J. Simonsz, "A finite-element analysis model of orbital biomechanics," *Vision Research*, vol. 46, no. 11, pp. 1724–1731, May 2006. [Online]. Available: https://www.sciencedirect.com/science/article/pii/S0042698905006632

[50] H. J. Simonsz, "Force-length recording of eye muscles during local-anesthesia surgery in 32 strabismus patients," *Strabismus*, vol. 2, no. 4, pp. 197–218, Jan. 1994. [Online]. Available: http://www.tandfonline.com/doi/full/10.3109/09273979409035475

[51] T. W. Olsen, S. Sanderson, X. Feng, and W. C. Hubbard, "Porcine Sclera: Thickness and Surface Area," *Investigative Ophthalmology & Visual Science*, vol. 43, no. 8, pp. 2529–2532, Aug. 2002.

[52] S. Mariacher, P. Laubichler, M. Mariacher, J. Wendelstein, I. Fischinger, and M. Bolz, "Impact of baseline IOP, vacuum, and different docking mechanisms, and their interaction on IOP rise in femtosecond laser-assisted refractive and cataract surgery:," *Journal of Cataract & Refractive Surgery*, vol. 45, no. 12, pp. 1818–1825, Dec. 2019. [Online]. Available: http://journals.lww.com/10.1016/j.jcrs.2019.07.020

[53] B. Li, "Effect of Pneumatic Suction Ring Placement on Intraocular Pressure in Cats," *Ophthalmic Research*, vol. 33, no. 5, pp. 271–275, 2001. [Online]. Available: https://www.karger.com/Article/FullText/55680

[54] D. W. Abu-Hassan, T. S. Acott, and M. J. Kelley, "The Trabecular Meshwork: A Basic Review of Form and Function," *Journal of ocular biology*, vol. 2, no. 1, May 2014. [Online]. Available: https://www.ncbi.nlm.nih.gov/pmc/articles/PMC4209746/

[55] V. P, K. P, and R. M, "Anthropometric analysis of palpebral fissure dimensions and its position in South Indian ethnic adults." *Oman Medical Journal*, vol. 28, no. 1, pp. 26–32, Jan. 2013. [Online]. Available: http://europepmc.org/article/PMC/3562989

[56] "Product search detail | Storz Ophthalmic Instruments." [Online]. Available: https://www.storzeye.eu/our-instruments/instrument/detail//list/category/wire/

[57] A. Abass, A. Eliasy, B. Geraghty, M. Elabd, A. Hassan, and A. Elsheikh, "Effect of freezing and thawing on the biomechanical characteristics of porcine ocular tissues," *Journal of Biomechanics*, vol. 87, pp. 93–99, Apr. 2019.

[58] "MJF PA12 Plastic 3D Printing Material Information." [Online]. Available: https://www.shapeways.com/materials/multi-jet-fusion-pa12

[59] V. P. Nguyen and V. A. Ho, "Wet Adhesion of Soft Curved Interfaces With Micro Pattern," *IEEE Robotics and Automation Letters*, vol. 6, no. 3, pp. 4273–4280, Jul. 2021. [Online]. Available: https://ieeexplore.ieee.org/document/9382855/

[60] M. Gerber, Y.-H. Lee, T.-C. Tsao, J. Rosen, and J.-P. Hubschman, "Docking system to stabilize eyeball during intraocular surgery," US Patent US20 210 000 566A1, Jan., 2021. [Online]. Available: https://patents.google.com/patent/US20210000566A1/en?oq=:+US+2021%2f0000566